JOURNAL OF THERMOPHYSICS AND HEAT TRANSFER
Vol. 11, No. 3, July–September 1997

Heat Transport Enhancement of Monogroove Heat Pipe with Electrohydrodynamic Pumping

J. E. Bryan* and J. Seyed-Yagoobi†
Texas A&M University, College Station, Texas 77843-3123

The enhancement of the heat transport capacity of a monogroove heat pipe with electrohydrodynamic (EHD) pumping was investigated. The EHD pump was located on the liquid channel in the adiabatic section of the heat pipe. The heat pipe fluid used in all experiments was R-123, a new alternative refrigerant. The two experimental goals were to determine the magnitude of heat transport enhancement that could be achieved using the EHD pump and to demonstrate the controllability and recovery of the heat pipe during dryout. Both were successfully accomplished. Over 100% enhancement in the transport capacity was achieved using the EHD pump operating at 20 kV. This enhancement could be maintained with less than 0.08 W of electric power to the EHD pump. The EHD pump was also able to provide immediate recovery from dryout when the heat pipe had been experiencing progressive evaporator dryout for over 70 min at 400 W.

Nomenclature

$\boldsymbol{E}$ = electric field
f_e = electric body force density
q = electric charge density
ε = fluid electric permittivity
ρ = fluid density

Introduction

THE design and development process of the International Space Station has resulted in many significant changes to the active thermal control system. The baseline active thermal control system was to be a two-phase pumped loop using high-capacity monogroove heat pipe radiators as the heat rejection medium to space. However, both the two-phase pumped loop and heat pipe radiators had technological problems. Thus, the active thermal control system became a single-phase pumped loop with flow through radiators; a design very similar to the Space Shuttle active thermal control system.

The return to heat pipe radiators is planned for the evolution of the International Space Station. One proposed heat pipe candidate[1] is the electrohydrodynamic (EHD) assisted monogroove heat pipe. The EHD assistance has the potential to eliminate the original problem of premature evaporator dryout during startup and transient heat loading.[2] Also, of the proposed heat pipe radiator candidates, only the EHD-assisted heat pipe provides an overall mass savings, which is a prime NASA concern.[1]

In recent years, the enhancement of heat and mass transfer with the EHD phenomena has gained substantial interest, and significant increases in performance and rapid performance controllability have been demonstrated. The commercialization of EHD technology to selected applications is expected to occur in the near future, particularly in the air conditioning and refrigeration industry.

The work presented in this paper focuses on the demonstration and performance assessment of a monogroove heat pipe augmented with EHD pumping. A few other researchers have also investigated enhancing heat pipe performance with the EHD phenomena. However, a better understanding of electrohydrodynamics is needed before the details and results of this work and that of other researchers are presented. The EHD phenomena involves the interaction of electrical fields and flowfields in a dielectric fluid medium. This interaction can result in electrically induced fluid motion that is caused by an electric body force. The electric body force density acting on the molecules of a dielectric fluid in the presence of an electric field consists of three terms[3]

$$f_e = q\boldsymbol{E} - \frac{1}{2}E^2\nabla\varepsilon + \frac{1}{2}\nabla\left[E^2\left(\frac{\partial\varepsilon}{\partial\rho}\right)\rho\right] \qquad (1)$$

The three terms in Eq. (1) stand for three different kinds of force densities acting on the fluid. The first term represents the coulomb force, which is the force acting on the free charges in an electric field. The second term stands for the dielectrophoretic force, which is created by a local change of the permittivity in an electric field. A change in the permittivity occurs, for example, at the interface between a liquid and a vapor. The third term is called the electrostriction force. The electrostriction force occurs primarily when a nonuniform electric field is applied on a dielectric fluid. The dielectrophoretic force and the electrostriction force are both forces that act on polarized charges and are defined as polarization forces.

Figure 1 fundamentally illustrates how a nonuniform electric field in a dielectric fluid medium can generate fluid motion because of the presence of a charged or neutral body. In the nonuniform (or uniform electric field, Ref. 4), the charged body will move along the field lines and impart momentum to the surrounding fluid. The fluid motion in this case is a result of the coulomb force. However, in an electric field, a neutral body is polarized, becoming a dipole. One end of this dipole in a nonuniform electric field (Fig. 1) experiences a higher force than the other end, resulting in a net translation of the polarized body toward the higher electric field. The fluid motion induced by the translation of the polarized body is a result of the polarization forces.

An advantage exists for using the polarization forces over the coulomb force when pumping a single-phase liquid. First, by using the polarization forces there is no direct injection of free charges into the dielectric fluid medium. This eliminates the potential of fluid degradation caused by external charge injection. Second, the polarization forces are more efficient for generating pumping over the coulomb force because they con-

Received Nov. 15, 1996; revision received March 24, 1997; accepted for publication March 28, 1997.

*Graduate Research Assistant, Department of Mechanical Engineering.

†Associate Professor, Department of Mechanical Engineering.

sume less power as a result of the nature of the current flow in the dielectric fluid medium. For the polarization forces, current flow in a dielectric fluid is through ohmic conduction. However, current flow for the coulomb force is through ohmic conduction, charge convection, and/or ionic mobility, because free charges have been injected into the dielectric fluid medium.

EHD pumping has a number of advantages over other active techniques in enhancing heat pipe performance: 1) simple design, nonmechanical, and lightweight; 2) rapid control of enhancement; 3) suitable for special environments (space); 4) minimal power consumption; 5) applicable to single or two-phase flows; and 6) uniform pressure distribution across pumping section.

However, the implementation of the EHD phenomena to fluid dynamics and heat transfer introduces a complex interaction of many interdependent variables. These variables are 1) electrical and thermophysical fluid properties; 2) electrical field strength; 3) fluid medium, single or multi-phase; 4) geometry of application; 5) geometry and configuration of electrodes; 6) properties of electrodes and insulators; and 7) operating environment.

A few researchers have investigated enhancing heat pipe performance with the EHD phenomena. Jones[5] proposed replacing the capillary wick structure from the condenser to the evaporator with an EHD pump that utilized polarization forces to generate pumping. By mounting a high-voltage electrode axially from the condenser to the evaporator near the grounded heat pipe wall, several advantages over a capillary heat pipe were expected: 1) increased heat transfer enhancements with EHD; 2) 100% reliable priming and start-up of heat pipe; and 3) control of heat transport by controlling applied voltage. Jones and Perry[6] demonstrated this concept successfully, but the performance was poor compared to existing capillary driven heat pipes. This was attributed to a significant mismatch of the circumferential capillary groove and EHD pumping capabilities. Loehrke and Debs[7] improved the EHD heat pipe of Jones and Perry,[6] and were able to achieve equivalent thermal throughputs of conventional axial-groove heat pipes at an adverse tilt of 1.7 cm compared to only 0.3 cm for the conventional heat pipe.

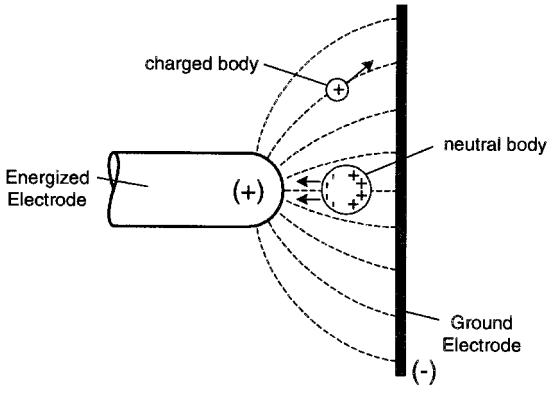

Fig. 1 Force on bodies in a nonuniform electric field.[4]

More recently, Bologa and Savin[8] used the dielectrophoretic force to enhance the heat transport capacity in an experimental heat pipe operating as a two-phase thermosiphon. By enhancing the rate of condensation with EHD, the heat transport capacity was increased 53% at an applied voltage of 36 kV. Enhancement of the heat pipe transport capacity utilizing the coulomb force was investigated by Babin et al.[9] They used an ion-drag pump to generate the coulomb force and to increase the capillary limit of the heat pipe. Using R-11 as the working fluid and a two-stage ion-drag pump located in the liquid passage, a 20% increase in the transport capacity was achieved at an applied voltage of 20 kV. Sato et al.[10] proposed using the electrostriction force to generate pumping to increase the heat pipe capillary limit, but did not provide any experimental evidence.

For the present work, as stated earlier, the heat transport enhancement of a monogroove heat pipe with an EHD pump utilizing the polarization forces is investigated. Using a monogroove heat pipe and configuration similar to the Space Station Heat Pipe Advanced Radiator Element (SHARE),[11] the heat transport enhancement, control, and EHD pump electric power consumption were measured.

Experimental Apparatus

A drawing of the EHD-assisted monogroove heat pipe used in this work is shown in Fig. 2. This heat pipe was built in a similar configuration to the SHARE (Ref. 11), to closely simulate a heat pipe configuration that could be used on the space station. The evaporator and adiabatic sections are approximately the same length as the SHARE unit, 66 cm and 84 cm, respectively. The separation of the liquid and vapor channel is also the same as the SHARE unit. The SHARE condenser was 640 cm long and the condenser in this work was 185 cm long. The shorter condenser was used because of laboratory space. The screens to aid in fluid wicking were removed from the heat pipe extrusions. A cross section of the evaporator and condenser extrusions are shown in Fig. 3. The extrusions are made of 6061-T6 aluminum. Both the evaporator and condenser extrusions had the same circumferential wall wick thread pattern in the vapor artery. Figure 3 shows the average measurements of the wall wick geometry taken from two samples of the heat pipe extrusions.

The heat pipe fluid used in all experiments was R-123, a new alternative refrigerant. R-123 was chosen because it was

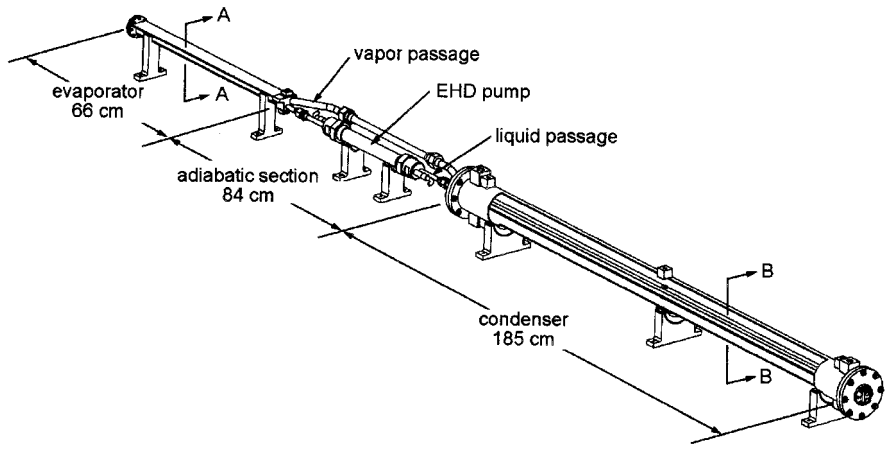

Fig. 2 Drawing of experimental monogroove heat pipe with EHD pump.

easy to use in the laboratory and it has produced good results in other EHD experiments. The results presented in this work are specific to R-123. Other fluids will produce different results because of the difference in electrical properties.

Heat was supplied to the evaporator along the top surface (Fig. 3) by four independently controlled 500-W strip heaters that were epoxied to the aluminum surface. Each heater was 16.2 by 5.1 cm (6.38 by 2.00 in.). They were mounted end-to-end and covered 98% of the evaporator length. In all experiments, the same power was supplied to each heater. The evaporator temperatures were monitored by platinum surface resistance temperature detectors (RTDs); 18 total: 9 for vapor and 9 for liquid located on the evaporator surface as shown in Fig. 3.

The heat was removed from the condenser (Fig. 3) with a water jacket that was connected to a recirculating chiller. The water inlet was at the end of the condenser and the outlet was at the beginning of the condenser. The water mass flow rate was 0.06–0.12 kg/s. The R-123 liquid and vapor temperatures were measured by RTDs located on the condenser surface (Fig. 3) at 7.6, 91.0, and 173.0 cm from the beginning of the condenser. For all experiments, the condenser heat flux was relatively uniform over the first half of the condenser, and the surface RTD readings on the vapor artery dropped no more than 1°C over 91 cm. However, at the highest heat load, the surface RTD readings on the vapor artery dropped just over 10°C from 91.0 to 173.0 cm. Thus, the effective transport length was greater than half the condenser, but less than the full length.

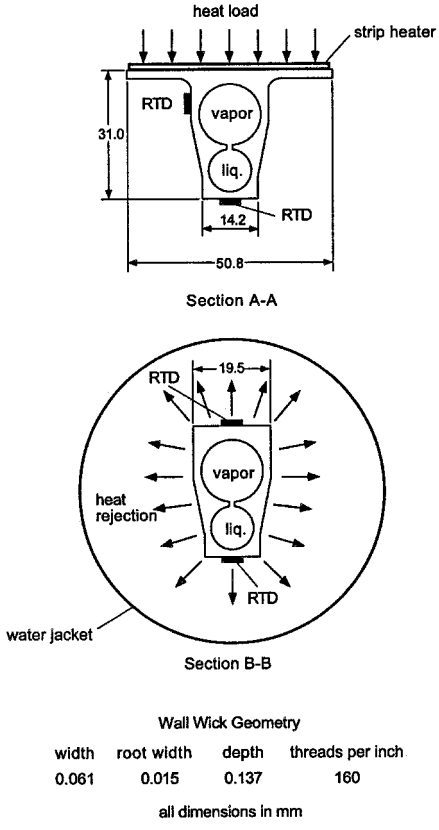

Fig. 3 Schematic of evaporator and condenser heat pipe extrusions.

The vapor temperature was also monitored at the exit of the evaporator and entrance of the condenser with T-type thermocouple probes. The pressure was measured at both ends of the heat pipe via absolute pressure transducers. To minimize heat loss to the surroundings, the entire experimental apparatus was first wrapped with a 2-cm-thick layer of Nomex™ insulation, and then wrapped with a 2-cm-thick layer of Rubatex™ insulation. The maximum heat loss from the evaporator to ambient was approximately 6% at 840 W at the 35°C chiller set point.

The EHD pump was connected to the liquid passage of the adiabatic section, where it would provide an increase in the liquid pressure head to the evaporator. The inner diameter of pump was 1 cm, which was the same as the liquid artery on the evaporator and condenser. The EHD pumping section consisted of six electrode pairs (six stages), as shown in the schematic in Fig. 4. The electrodes were designed to generate a very nonuniform electric field distribution and prevent charge injection. It should be noted that the electrodes were by no means optimized; this electrode geometry was used because it provided an adequate nonuniform electric field. This EHD pump is believed to utilize the polarization forces for two specific reasons. First, the pumping direction achieved with this pump was opposite to the pumping direction that would be achieved by an EHD pump driven by the coulomb force. Second, under steady-state operation, the current level of the EHD pump used in this study is at least an order of magnitude smaller than the current level expected if the coulomb force was present.

The heater power was determined from the applied voltage and current, and the removed heat was determined from the flow rate and inlet and outlet temperatures from the water jacket. The EHD pump power was determined from the applied voltage and input current. The accuracy of temperature and pressure measurements were ±1°C and ±2 kPa, respectively. The maximum uncertainty in the heater power was ±0.37 W (occurred at 840 W). The maximum uncertainty in the EHD pump electric power was ±1.1 mW (occurred at 0.02 W). To test the heat pipe at different adverse tilts, an electrically activated lead screw was used. The level of the heat pipe and the height of the adverse tilt were measured with a surveyor's level. The accuracy of the measurements were within ±0.13 mm.

In all experiments the repeatability of the heat transport capacity was within ±1%. However, there are two variables that need to be addressed. First, the heat load increments were 40 W (10 W per heater), which corresponds to 5% of the highest transport capacity achieved (840 W), indicating a relatively

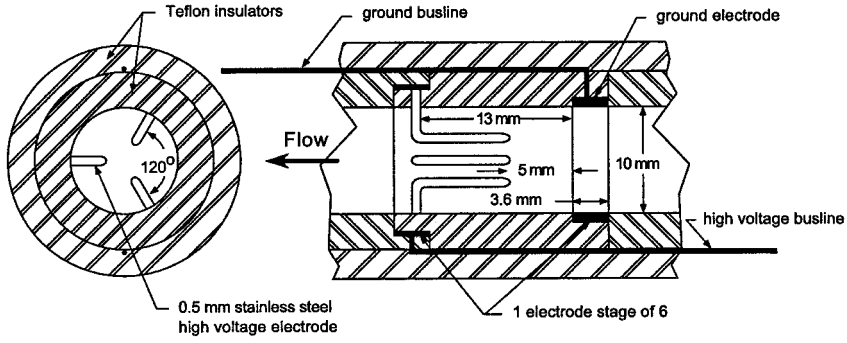

Fig. 4 Schematic of electrode stages used in EHD pump.

large increment. The second variable affecting the heat pipe performance was the heat pipe charge, the performance was found to be very sensitive to charge. With the existing charging procedure it was hard to precisely match the charge of the heat pipe each time it was changed. Because of this, the heat transport capacity varied to some degree among different runs. However, the charge inventories never differed by more than 6% and the charge was always adequate for proper heat pipe operation.

Experimental Procedure

All experiments were started by setting the chiller set point temperature that established the heat pipe condenser environment and by setting the heat pipe to 0-mm adverse tilt. Heaters were turned on once the chiller reached the set point temperature and the heat pipe reached steady state (the time to reach this point varied from an hour to several hours, depending on the chiller set point). Heat was uniformly applied to each of the four heaters in 10-W increments (40 W total) with no power applied to the EHD pump. Power to heaters was increased once the average evaporator vapor and liquid temperatures reached steady state, which was about 10–15 min. The increase in heat load to the evaporator continued until dryout began. Dryout was easily detected by monitoring the average vapor and liquid evaporator temperatures that would continue to rise (this will be seen on a time line plot that will be presented and discussed in the results section). The EHD pump was then turned on with 10 kV applied dc voltage once the dryout was detected. When steady state was reached the heat load was again increased in 40-W increments. This was continued until the heat pipe began to dry out for the second time, at which time the applied dc voltage to the EHD pump was increased to 20 kV and the heat load was again increased in 40 W increments. Once the heat pipe dried out with the EHD pump at 20 kV, all heaters were reduced to 0 W and the heat pipe was returned to 0 mm adverse tilt. When the heat pipe reached steady state, the adverse tilt was changed and the previous procedure was repeated.

Additional experiments were also performed to study the control and dryout recovery of the heat pipe using the EHD pump. In these experiments the time between increases in heat load was longer and the heat load increments were larger to evaluate various characteristics of the heat pipe operating with the EHD pump.

Results and Discussion

The first experimental goal was to determine the magnitude of heat transport enhancement that could be achieved using the EHD pump. Experiments of the EHD-assisted monogroove heat pipe produced some excellent results (Figs. 5a and 5b). At a 5°C chiller set point and 0-mm adverse tilt, the heat transport capacity (prior to dryout) was increased 86 and 114% at 10 and 20 kV, respectively. At a 35°C chiller set point and 0 mm adverse tilt, the heat transport capacity was increased 50 and 110% at 10 and 20 kV, respectively. The results are very promising, considering that the electrode design for the pump is not optimized. There are a few additional observations in Figs. 5a and 5b that should be discussed. First, the heat pipe transport capacity is greater at the 35°C set point at all EHD pump voltages (including 0 kV) over the 5°C setpoint at 0-mm adverse tilt. This result is expected and is common for monogroove heat pipe operation, and it is caused by the temperature dependence of the fluid thermal properties. However, the heat pipe operating temperature has a small effect on the EHD pump performance, which is only increasing the liquid supply pressure head. The second observation was that the slope of the data for the 5°C set point was not as steep as the data for the 35°C set point. Also, at both set points, no heat transport could be achieved with the EHD pump above 21 mm adverse tilt. The increase in enhancement from 0 to 10 kV and 10 to 20 kV for the 35°C set point was almost even at each

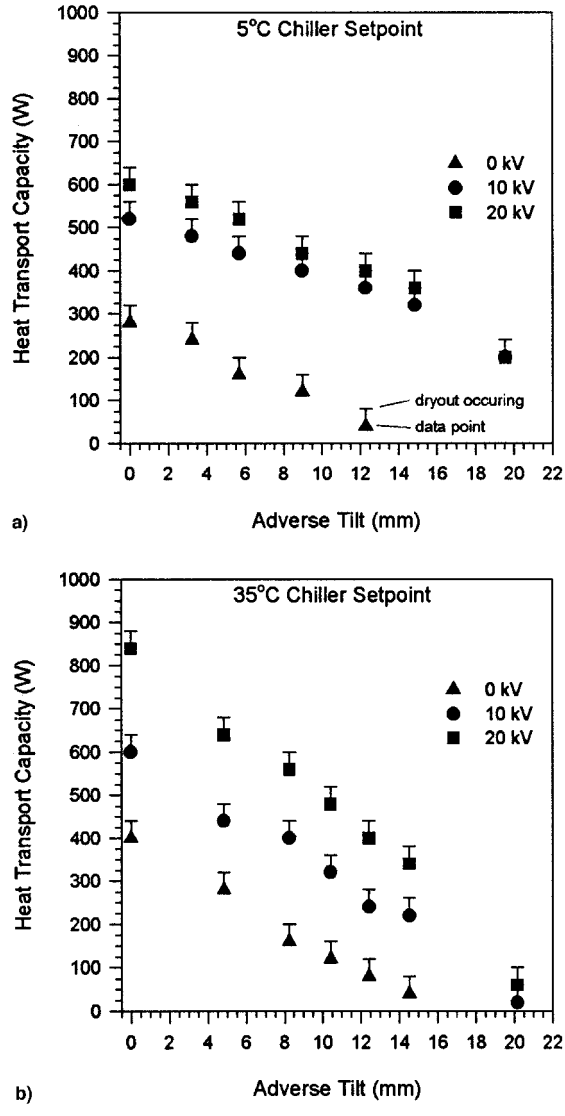

Fig. 5 Heat transport capacity vs adverse tilt for a) 5°C and b) 35°C chiller set points.

adverse tilt, but at the 5°C set point the increase in enhancement was greater from 0 to 10 kV than from 10 to 20 kV for all adverse tilts. The heat pipe charge for the 35°C set point test series was 5.5% less than the charge for the 5°C set point test series. However, the specific volume of R-123 increased 4% for the 35°C test series.

The heat transport capacity of the heat pipe reaches a limit when the capillary wicking structure fails to pump enough fluid from the condenser to the evaporator to maintain continued operation. The capillary pumping pressure can be increased by incorporating the EHD pump into the heat pipe. The pressure head generated by the EHD pump was not measured; however, the capillary and EHD pressure heads could be approximately determined. For example, the pressure head was extrapolated from the heat transport data for the adverse tilt at 0 W heat transport capacity in Fig. 5b, and was just the static pressure head that was approximately 210, 260, and 320 Pa at 0, 10, and 20 kV, respectively. The previous values provide an estimate of the increase in pressure head provided by the EHD pump, but to accurately determine the EHD pump capabilities, the pressure head should be properly measured.

The input current to the EHD pump as a function of heat transport is important in determining the power cost for achieving the enhanced heat transport capacity with the EHD pump. Thus, the input current to the EHD pump was measured vs time and with respect to heat transport at the two different

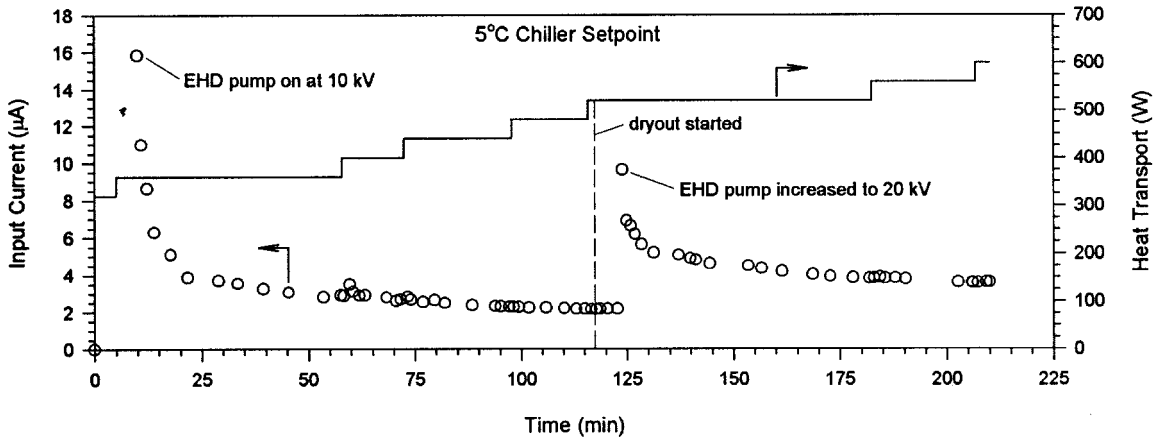

Fig. 6 Time line of input current to the EHD pump for heat pipe operating at 5°C chiller set point.

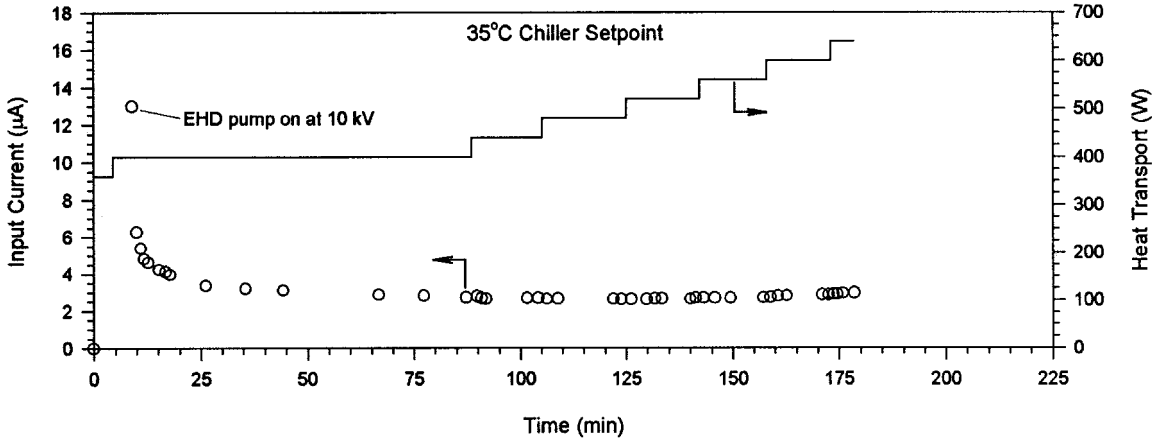

Fig. 7 Time line of input current to the EHD pump for heat pipe operating at 35°C chiller set point.

chiller set points (Figs. 6 and 7). For Fig. 6, at 0 mm tilt and 5°C chiller set point, the data shown were the measured input current from the point dryout started at 360 W, and the EHD pump was turned on to 10 kV to the point dryout started at 600 W with the EHD pump operating at 20 kV. For Fig. 7, at 0 mm tilt and 35°C chiller set point, the data shown were the measured input current from the point dryout started at 400 W, and the EHD pump was turned on to 10 kV to the point dryout started at 640 W.

The current settling time is a function of the electrical characteristics of R-123, as well as the temperature of the heat pipe. As the operating temperature of the heat pipe increases, the conductivity of the fluid increases, thus increasing the current slightly. With the EHD pump operating at 10 kV, the current settled to 2.2 μA at 5°C set point and 2.7 μA at 35°C set point. It is very interesting to note that the ratio of the electric conductivities of R-123 at the two chiller set point conditions (2.46×10^{-8} S/m at 5°C set point and 3.07×10^{-8} S/m at 35°C set point) is almost equal to the ratio of the settled current values. This indicates that ohmic conduction is the prime mechanism for electric current flow within the EHD pump, and is a further indication that the EHD pump used in this study is driven by the polarization forces and not the Coulomb force. Also, because the current is so low there is negligible Joule heating (ohmic dissipation).

In both Figs. 6 and 7, the current settling time takes over 100 min and does not appear to be affected by an increase in the heat transport (note: the increase in heat transport is achieved by increasing the power to the evaporator heaters). At 10 kV and 5°C set point, the peak measured power to the EHD pump was only 0.16 W and settled to 0.02 W, and at 10 kV and 35°C set point the peak measured power to the EHD pump was only 0.13 W and settled to 0.03 W. At the 5°C set point and 20 kV, the peak measured current corresponded to only 0.19 W power to the EHD pump, and to 0.07 W once the current settled. Note that the current behavior and settling time will be different for different fluids.

The second experimental goal was to demonstrate the controllability and recovery of the heat pipe during dryout. To do this the heat transport limit was determined at 0 mm adverse tilt at the 5°C set point with no EHD. Then the heat pipe was operated at a heat load below and above the heat transport limit, and without and with the EHD pump to study the control and recovery of the heat pipe. A time line of this study with the average evaporator vapor and liquid temperatures, the pump input current, and average heat pipe pressure are shown in Figs. 8 and 9, respectively. There are several observations that can be made from these figures, but the most important one is the EHD pump's ability to provide immediate recovery from dryout. This can be seen from two different points on the time line in Fig. 8. The first point is when the pump is turned on to 15 kV after the heat pipe had been drying out for over 25 min because of a heat load increase from 240 to 400 W with no EHD. The second point is when the pump is turned on to 20 kV after the heat pipe had been drying out for almost 70 min at 400 W with no EHD. At both points where the EHD pump is turned on, the heat pipe immediately begins recovery from dryout, which is a result of the immediate increase in the liquid pressure head supplied by the EHD pump. The EHD pump recovered the evaporator temperature in about 17 min from a state where well over one-half of the evaporator contained no liquid (Fig. 10). In Fig. 8, time is just before the

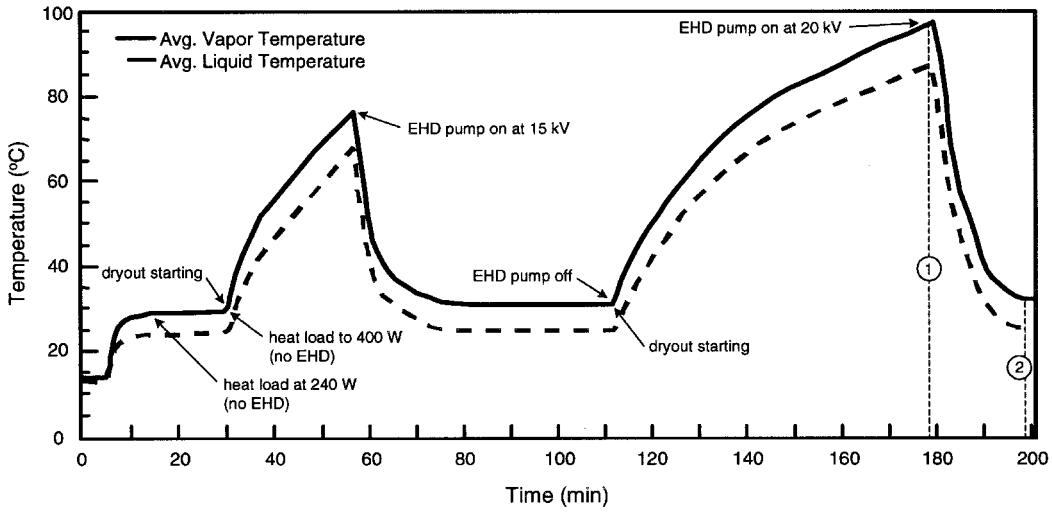

Fig. 8 Time line depicting the average evaporator vapor and liquid temperatures for 5°C chiller set point.

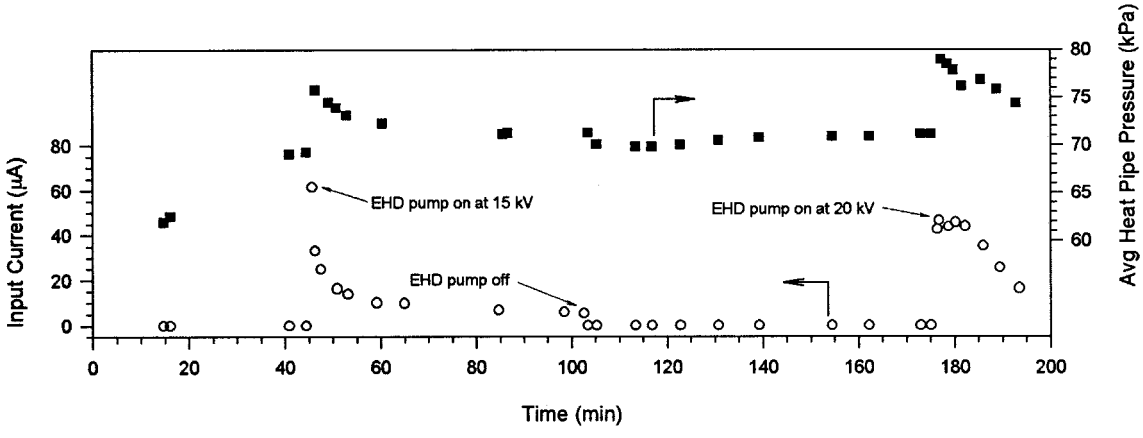

Fig. 9 Time line of input current to the EHD pump and average heat pipe pressure corresponding to Fig. 8 time line.

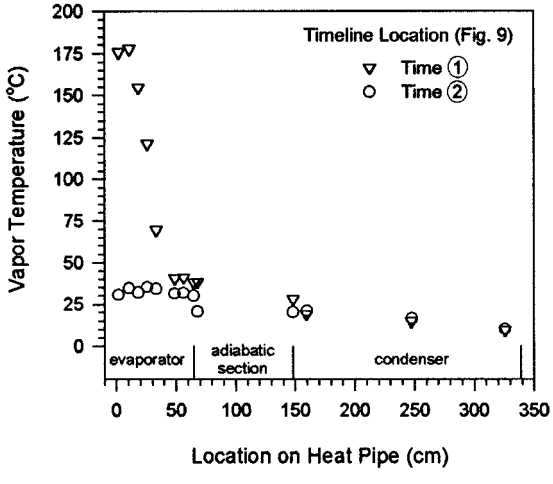

Fig. 10 Vapor temperatures along the heat pipe at two different times as shown in Fig. 8.

EHD pump is turned on, and time is 17 min later when all of the evaporator temperatures are about to reach steady state. Only 0.9 W peak power (occurs at current spike) is used to generate this rapid recovery, and this power is only 0.23% of the total heat transport (less than 0.08 W is used to maintain the 400-W heat transport).

A few other interesting observations were also made. First, as the heat pipe dried out, the evaporator heated up and did not transport the heat to the condenser, and since the apparatus was well insulated, the heat was stored in the evaporator. The EHD pump not only recovered the evaporator, but it transported this stored heat. This is seen in Fig. 9 when the EHD pump was turned on and the pressure spiked and then slowly settled (pressure was measured at the end of the evaporator and the condenser). The second observation was that the input current spike was also much higher in Fig. 9 than those in Figs. 6 and 7. The third observation worth noting was that the steady-state heat pipe operation at 400 W with the EHD pump operating at 15 kV was practically isothermal (Table 1). However, the heat pipe operation at 240 W without the EHD pump operating was not isothermal. This is interesting considering the average heat pipe pressure increased 15% (Fig. 8) between 240–400 W heat transport. Thus, even with the heat pipe operating at 400 W, the EHD pump is providing a surplus of liquid to the evaporator to maintain isothermal operation. If the heat pipe was operating in a microgravity environment, the EHD pumping head would have to be controlled, otherwise, the condenser meniscus could be broken and vapor could be drawn into the liquid artery, thus depriming the evaporator.

Table 1 Heat pipe operating conditions

EHD, kV	Heater power, W	Vapor temperature, °C: Evaporator exit	Vapor temperature, °C: Condenser inlet	P_{sat}, kPa	T_{sat}, °C
0	240	21.1	17.2	62.0	15.0
15	400	18.9	18.9	71.3	18.6

Conclusions

An EHD pump was successfully implemented into a monogroove heat pipe whose configuration was similar to the SHARE heat pipe that had been a heat pipe radiator design option for the International Space Station. Over 100% enhancement in the heat transport capacity was demonstrated as well as the EHD pump's ability to provide immediate recovery from dryout. This performance enhancement and controllability was achieved using the polarization forces and electrodes that were far from optimized.

Acknowledgments

The authors gratefully acknowledge the support of this research by NASA Johnson Space Center (NASA–JSC). The authors also gratefully acknowledge Katherine Miller-Hurlbert, NASA–JSC, for program support, and Gale Hanson, Lockheed Martin Corp., for technical support for the maintenance and operation of the experimental apparatus.

References

[1]Hanford, A. J., and Ewert, M. K., "Advanced Active Thermal Control Systems Architecture Study," NASA TM 104822, Houston, TX, Oct. 1996.

[2]Kosson, R., Brown, R., and Ungar, E., "Space Station Heat Pipe Advanced Radiator Element (SHARE) Flight Test Results and Analysis," AIAA Paper 90-0059, Jan. 1990.

[3]Melcher, J. R., *Continuum Electromechanics*, MIT Press, Cambridge, MA, 1981.

[4]Pohl, H. A., *Dielectrophoresis*, Cambridge Univ. Press, Cambridge, MA, 1978.

[5]Jones, T. B., "An Electrohydrodynamic Heat Pipe," *Mechanical Engineering*, Vol. 96, No. 1, 1974, pp. 27–32.

[6]Jones, T. B., and Perry, M. P., "Electrohydrodynamic Heat Pipe Experiments," *Journal of Applied Physics*, Vol. 45, No. 5, 1974, pp. 2129–2132.

[7]Loehrke, R. I., and Debs, R. J., "Measurements of the Performance of an Electrohydrodynamic Heat Pipe," AIAA Paper 75-659, May 1975.

[8]Bologa, M. K., and Savin, I. K., "Electrohydrodynamic Heat Pipes," *Proceedings of the 7th International Heat Pipe Conference* (Minsk), Begell House, New York, 1990, pp. 549–562.

[9]Babin, B. R., Peterson, G. P., and Seyed-Yagoobi, J., "Experimental Investigation of an Ion-Drag Pump Assisted Heat Pipe," *Journal of Thermophysics and Heat Transfer*, Vol. 7, No. 2, 1993, pp. 340–345.

[10]Sato, M., Nishida, S., and Noto, F., "Study on Electrohydrodynamical Heat Pipe," *ASME JSES KSES International Solar Energy Conference, Part 1 of 2*, American Society of Mechanical Engineers, New York, 1992, pp. 155–160.

[11]Brown, R., Ungar, E., and Cornwell, J., "Flight Test Results of the SHAREII Monogroove Heat Pipe," AIAA Paper 92-2886, July 1992.